Long-range order near the $Cu_3Au(001)$ surface by evanescent x-ray scattering

H. Dosch, L. Mailänder, H. Reichert, and J. Peisl
Sektion Physik der Universität München, D-8000 München 22, Germany

R. L. Johnson
II. Institut für Experimentalphysik der Universität Hamburg, D-2000 Hamburg 50, Germany
(Received 26 July 1990)

We present an experimental study of the surface effects on the order-disorder phase transition in the binary alloy Cu_3Au. By x-ray scattering under the condition of total external reflection, we obtained depth profiles of the order parameter at the (001) surface when the transition temperature T_0 is approached. The scattered intensity is analyzed in the framework of the distorted-wave Born approximation, which is briefly outlined. The temperature and depth dependence of the evanescent (100) superlattice intensity is consistent with a wetting transition, which is driven by the first-order bulk transition: Close to T_0 the disordered phase appears at the (001) surface and grows according to $L(t)=(13.1\ \text{Å})\ln|1/t|$ with reduced temperature t. During these measurements the near-surface Debye-Waller factor was monitored via the (200) evanescent Bragg intensity, which, however, showed no significant surface effects at T_0. In several temperature quench experiments, where the system was rapidly cooled from $T > T_0$ to $T_0-\Delta T$, we measured time- and depth-resolved evanescent superlattice intensities. We present depth-resolved near-surface relaxation times that exhibit a very distinct depth dependence. A first quantitative analysis of the relaxation processes is indicated and gives results consistent with the assumption of an ordinary "surface-induced disorder."

I. INTRODUCTION

Surfaces and interfaces modify bulk order-disorder phase transitions in a fundamental manner: Since the atoms at the surface of solids are less tightly bound than their counterparts in the bulk, long-range order (LRO) may be slightly reduced at the surface. In this case the interface favors the disordered phase and facilitates the surface regime to reach the disordered state. The characteristic feature of such phenomena is that the surface effects are not two-dimensional, i.e., they are not simply confined to the surface; there is a continuous spatial transition regime from the surface-modified behavior to the pure bulk behavior as one moves from the surface into the interior of the system, the length scale of this transition being determined by the correlation length ξ of the matter. Since ξ diverges at a critical point, it has been the general wisdom for some time that the action of the surface only becomes spectacular when the system approaches its critical temperature. In the last decade it became apparent that first-order phase transitions are also fundamentally altered close to the border of a system, where surface-induced critical phenomena may occur which are completely absent in the bulk. The transition regime between the two-dimensional surface and the three-dimensional bulk then mediates between a critical surface and a noncritical bulk.

In this paper we present experimental studies of the long- and short-range order associated with this near-surface regime in the binary alloy Cu_3Au which undergoes a discontinuous order-disorder ($L1_2 \Longrightarrow A2$) transition at $T_0=663$ K. By studying the properties of the LRO parameter near the (001) surface in thermal equilibrium and upon a temperature quench, we obtained strong experimental evidence that this surface acts as a natural nucleus for the disordered phase. When T_0 is approached from the ordered state, the thickness of this surface-induced disordered phase grows and "wets" the surface in close analogy to the surface melting phenomenon. In fact, the first-order transition in this system may be regarded as a model for a particularly simple melting process, where, in contrast to conventional melting, only one Fourier component of the system vanishes. Thus, the disorder wetting observed in this alloy can be viewed as a surface-melting process of an Ising system.

In order to obtain information on the near-surface long-range order, we applied a novel x-ray-scattering technique. As one knows, conventional x-ray scattering is a bulk technique, however, it can be rendered surface sensitive by exploiting the effect of total external reflection which occurs at very grazing incidence angles (with respect to the surface). While the classical surface-sensitive tools like low-energy electron diffraction (LEED), its spin-polarized version (SPLEED), or low-energy ion scattering (LEIS) exclusively probe the structure and chemical composition of the top and second layer, x-ray scattering at grazing angles can be used to obtain depth profiles of the short- (SRO) and long-range order between some 10 Å and several 100 Å near the surface under investigation. The depth of the probe can be tuned within this mesoscopic range rather simply by varying the grazing angles which determine the decay length of the evanescent wave field inside the sample.

This external depth control, together with a straightforward semikinematic interpretation of the evanescent scattering, make grazing-angle diffraction of x rays ideally suited to the investigation of phenomena between two and three dimensions. The potential of this technique to study surface-induced critical scattering in binary alloys has recently been demonstrated using intense x-ray synchrotron radiation.[1,2]

This paper is organized as follows: In Sec. II we briefly summarize the theoretical and experimental situation in the understanding of the LRO parameter and its temperature dependence in the bulk and at the surface of Cu_3Au. Before discussing our experimental results on the (001) surface, we outline the framework of the distorted-wave Born approximation (DWBA) (Sec. III) and give some information on the experimental details on the scattering geometry and the sample preparation and characterization procedure (Secs. III and IV). The presentation of the experimental results is divided into two parts: Measurements of depth profiles of the near-surface superlattice intensity in thermal equilibrium and the interpretation in terms of a wetting transition are found in Sec. V. In complementary experiments we performed temperature quenches at various temperature conditions and scattering geometries and observed the time dependence of the depth-resolved grazing-angle scattering (Sec. VI).

II. THE ORDER PARAMETER IN Cu_3Au

The bulk phenomena in Cu_3Au associated with the order-disorder transition at $T_0=663$ K have been meticulously studied by the pioneers in the field: Warren,[3] Cowley,[4] Moss,[5] Chipman,[6] and others. Thus, surface experiments on this alloy can be based on an exceptionally well-understood bulk reference.

The ordered alloy exhibits an $L1_2$ structure with four simple-cubic sublattices, where three of them (α sites) are occupied by Cu and one (β sites) by Au atoms (Fig. 1). Accordingly, the Bragg-Williams long-range order parameter is defined as[4]

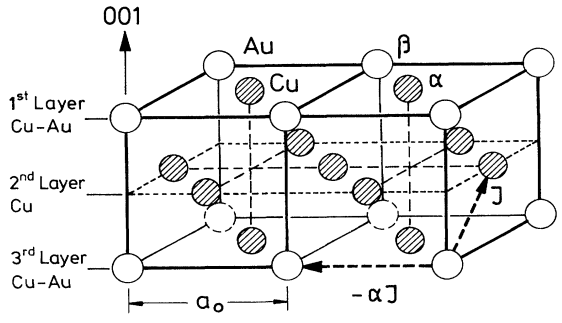

FIG. 1. Structure of the ordered Cu_3Au crystal. $a_0=3.75$ Å is the lattice constant, J and $-\alpha J$ are the NN and NNN interactions. The (001) surface and the associated near-surface layers are indicated.

$$m=\frac{3}{4}\left[\frac{r_\alpha-c_{Cu}}{1-c_{Cu}}\right]+\frac{1}{4}\left[\frac{r_\beta-c_{Au}}{1-c_{Au}}\right] \quad (1)$$

with r_α and r_β as the fractions of the correctly occupied sites which range from 1 in the ordered state to c_{Cu} and c_{Au}, respectively, in the disordered state (c_{Cu}, c_{Au} are the Cu and Au concentrations). It is well known that an $L1_2$ structure cannot have a simple Ising ground state, if only "antiferromagnetic" interactions ($J>0$) between the 12 nearest neighbors (NN) are taken into account; thus, in order to remove the frustrated "$T=0$" configuration, at least a competing "ferromagnetic" interaction among the 6 next-nearest-neighbors (NNN) is required, resulting in a Hamiltonian

$$H=J\sum_{NN}\tau_i\tau_j-\alpha J\sum_{NNN}\tau_i\tau_j\ ,$$

where $\tau_i=\pm1$, when site i is occupied by Cu and Au, respectively, and $\alpha=0.2$ (Ref. 7). As a consequence of this interlocked competing interaction, long-range order in Cu_3Au does not disappear continuously upon approaching T_0, but instead, the order-disorder transition has been found by various x-ray-scattering studies to be very pronounced first order.[4,8,9]

At and near a free surface, the atoms have a different, no longer close-packed, local environment, e.g., the atoms belonging to the top layer of the (001) surface (see Fig. 1) have only 8 NN and 5 NNN (compared to 12 NN and 6 NNN in the bulk), and may therefore show a different ordering behavior. Such a surface-induced effect on the long-range order has indeed been discovered by LEED at the $Cu_3Au(001)$ surface: the top layers display a continuous order-disorder transition,[10–13] whereby the surface order parameter m_1 obeys a power-law $M_1=|t|^{\beta_1}$ with $\beta_1=0.77$ [$t\equiv(T_0-T)/T_0$ is the reduced temperature]. Sanchez and Moran-Lopez[14] analyzed an effective Hamiltonian of a semi-infinite fcc A_3B alloy with the cluster-variation method and essentially reproduced the observed continuous behavior of m_1 at the (001) surface, if the surface pair interaction $J_s=0.72J$ (J is the bulk value). Within this approach, the continuous behavior of m_1 appears as a two-dimensional transition of a weakly coupled surface layer. A completely new insight into these kind of surface phenomena was provided by Lipowsky and co-workers[15–18] who suggested that the continuous behavior of m_1 is mediated by a wetting phenomenon driven by the discontinuous bulk phase transition: When the free surface of the ordered alloy favors disorder, an order-parameter profile $m(z)$, as shown in Fig. 2(a), may develop at temperatures well below T_0. Within mean-field theory, it is straightforward to show that such a situation will finally lead to the emergence of a disordered surface layer to microscopic thickness $L(t)$ [Fig. 2(b)], which can grow to a mesoscopic and even macroscopic size when T_0 is approached. This entails a continuous temperature dependence of the surface order parameter m_1 with the universal quantity $\beta_1=0.5$. As long as short-range interactions dominate the surface phenomena, one expects this wetting layer to grow according to

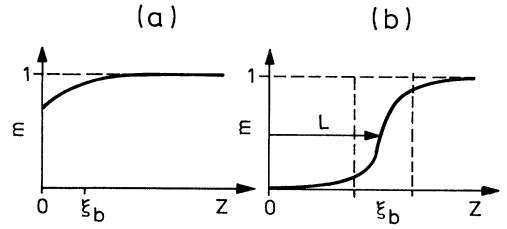

FIG. 2. Long-range-order profiles close to the free surface. $z=0$ denotes the surface. (a) $T \ll T_0$, onset of surface disorder; (b) $T < T_0$, disordered surface layer with thickness L. The thermal roughness of the interface is ξ_b.

$$L(t)=\xi_d \ln(1/t) , \tag{2}$$

where ξ_d is the correlation length in the disordered phase (which remains finite at all temperatures). However, this simple universal wetting scenario is, in general, not observable in binary alloys, because the broken bonds at the surface usually lead to surface segregation effects. This, in turn, may modify the surface-induced critical behavior drastically. The competition between ordering and nonordering at the surface of A_3B systems renders the nature of the wetting transition rather complex,[19] i.e., it depends particularly sensitively on the symmetry of the system and of the surface and on the range and type of the interactions. The surface composition in the first and second layer of the $Cu_3Au(001)$ has been measured by LEIS below and above the bulk transition temperature:[20] In the ordered state, the top layer is the Cu:Au-1:1 layer followed by a pure Cu layer and so forth (Fig. 1); thus, the (001) surface exhibits a segregation-free, ideal stoichiometric termination. The remarkable observation is that this layering remains unchanged at temperatures far beyond T_0. Apparently, the order-disorder transition is not associated with an interdiffusion of the atoms between near-surface layers, a fact which has some important consequences, e.g., first, during ordering and disordering no long-range diffusion processes are involved (we come to this later in Sec. VI), and second, the near-surface short-range order above T_0 must be consistent with this layered structure. Theoretical values for the surface exponent β_1 deduced from a two-density mean-field theory and from Monte Carlo calculations[19] accounting for the layer composition range from 2.22 to 1.72 depending on the actual role of the interfacial fluctuations which is not yet well understood.[21] At any rate, this range for β_1 is in clear contradiction to the experimental value[13] $\beta_1=0.77$, which, to add to the confusion, seems to agree more with the predictions of a mean-field approximation (MFA) theory which discards the action of nonordering densities.[18] This was the state of the understanding of the LRO at the $Cu_3Au(001)$ surface, when the x-ray experiments described below were initiated.[1] The particularly intriguing question to answer was whether an experiment using evanescent x rays could not detect any indication of a wetting transition.

III. THEORETICAL AND EXPERIMENTAL ASPECTS OF EVANESCENT X-RAY SCATTERING

The basis of our experimental setup is depicted schematically in Fig. 3: A monochromatic and highly collimated x-ray beam (as provided by modern synchrotron light sources) impinges on the mirrorlike surface of the binary alloy whose average x-ray optical properties are given by the index of refraction

$$n=1-\delta-i\beta$$

with

$$\delta=\lambda^2 r_e \frac{N(Z-\Delta f')}{\pi} ,$$

$$\beta=\lambda\mu/4\pi$$

(μ=linear photoabsorption coefficient) .

λ is the wavelength of the radiation,

$$r_e=e^2/(4\pi\epsilon_0 mc^2)=2.814\times10^{-5} \text{ Å}$$

is the classical electron radius, N is the number density of the atoms with charge number Z, and $\Delta f'$ is the real part of the dispersion correction. In our case, for Cu_3Au and a wavelength of $\lambda=1.50$ Å, we have[22] $\Delta f'_{Cu}=-2.1$, $\Delta f'_{Au}=-5.0$, and $\beta=1.813\times10^{-6}$ resulting in a critical angle for total external reflection $\alpha_c=\sqrt{2\delta}=7.8$ mrad.

When the incidence angle α_i is close to α_c, the penetration depth of the transmitted wave into the medium is limited to some 50–100 Å and thereby allows the study of surface-related structural phenomena. Experimentally, we then observe a specularly reflected intensity at an exit angle $\alpha_s=\alpha_i$ and out-of-plane-of-incidence scattering from the evanescent wave field at a scattering angle $2\Theta_B$ and an exit angle α_f.

In DWBA, the scattering cross section $d\sigma/d\Omega$ of this scattering has the general form[23,24]

$$\frac{d\sigma}{d\Omega}(\mathbf{Q})=r_e^2|\mathbf{t}_{fi}|^2 S(\mathbf{Q}) , \tag{3}$$

where $|\mathbf{t}_{fi}|^2$ is a transmission-polarization factor which will be discussed later, and $S(\mathbf{Q})$ the semikinematic structure factor of the scattering process under consideration. In contrast to conventional bulk scattering, the z-component of the scattering vector Q'_z is a complex quan-

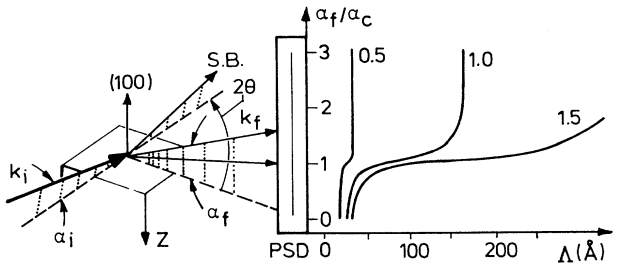

FIG. 3. Scheme of grazing-angle diffraction (see main text) and associated scattering depths in Cu_3Au as a function of α_f/α_c for $\alpha_i/\alpha_c=0.5$, 1.0, and 1.5.

tity in the half-space $z \geq 0$,

$$Q_z' = k_{iz}' - k_{fz}' \equiv q_z' + i/\Lambda \tag{4}$$

with the "evanescent wave vectors" for elastic x-ray scattering

$$(k_{if}')_z = \pm \frac{2\pi}{\lambda}(\sin^2\alpha_{if} - 2\delta - 2i\beta)^{1/2} . \tag{5}$$

The above structure factor,

$$S(\mathbf{Q}) = \sum_{\mathbf{r}_m} \sum_{\mathbf{r}_n} \langle \rho(\mathbf{r}_m)\rho(\mathbf{r}_n)\rangle e^{-i\mathbf{Q}\cdot\mathbf{r}_m + i\mathbf{Q}^*\cdot\mathbf{r}_n} \tag{6}$$

is the semi-infinite Fourier-Laplace transform of the density-density correlation function $\langle \rho(\mathbf{r}_m)\rho(\mathbf{r}_n)\rangle$ with the brackets $\langle\ \rangle$ indicating the ensemble average. The Laplace transformation in Eq. (6) with respect to the "scattering depth" $\Lambda = \mathrm{Im}^{-1}(Q_z')$ determines the depth profile of the scattering ranging from some 10 Å for α_i and α_f below α_c to several 100 Å at steeper incidence and exit angles (Fig. 3).

The geometric factor $|\mathbf{t}_{fi}|^2$, which accounts for the transmissivity of the surface and polarization effects, is not particularly interesting in this study, but has to be properly taken into account. One finds

$$|\mathbf{t}_{fi}^{\perp}|^2 = |T_{i2}|^2[\,|T_{f2}|^2\cos^2 2\theta + |T_{f1}|^2\sin^2 2\theta \sin^2\alpha_f\,], \tag{7}$$

$$|\mathbf{t}_{fi}^{\parallel}|^2 = |T_{i3}|^2|T_{f3}|^2 + (\,|T_{i1}|^2|T_{f2}|^2\sin^2 2\theta \sin^2\alpha_i + |T_{i3}|^2|T_{f3}|^2\sin^2\alpha_f - 2|T_{i1}T_{f1}T_{i3}T_{f3}|\cos 2\theta \sin\alpha_i \sin\alpha_f\,) \tag{8}$$

for the two cases of x-ray polarized normal ($\perp$) and parallel ($\parallel$) to the plane of incidence. For an ideal interface, the transmission coefficients $T_{a\sigma}$ ($a = i,f$; $\sigma = 1,2,3$) are given by the conventional interface equations[25]

$$T_{a1} = \frac{2\sin\alpha_a}{n^2\sin\alpha_a + \sin r\alpha_a} ,$$

$$T_{a2} = \frac{2\sin\alpha_a}{\sin\alpha_a + \sin r\alpha_a} , \tag{9}$$

$$T_{a3} = \frac{2\sin\alpha_a}{n^2\sin\alpha_a + \sin r\alpha_a} ,$$

where $\sin r\alpha \equiv (\sin^2\alpha - 2\delta - 2i\beta)^{1/2}$ denotes the "refracted $\sin\alpha$" in the medium.

In this study we consider LRO in a binary alloy, then $\langle \rho(z)\rangle \rightarrow m(z)$ is the depth profile of the Bragg-Williams LRO parameter which depends, because of the broken translational symmetry, on the distance z to the surface. The evanescent superlattice structure factor (6) is, accordingly, the Fourier-Laplace transform of $m(z)$.

The experiments were performed at the Hamburg Synchrotron Laboratory (HASYLAB) using synchrotron radiation from the DORIS II storage ring at Deutsches Elektronen-Synchrotron (DESY). The results described below were obtained during two experiments in the nondedicated operation mode of HASYLAB ($E = 5.2$ GeV, $I = 40$ meV): The measurement of the near-surface LRO has been performed on the D4 spectrometer using radiation from a bending magnet. The sample surface was mounted horizontally; thus, the incident beam is polarized perpendicular to the plane of incidence, and the transmission-polarization factor $|\mathbf{t}_{fi}^{\perp}|^2$ (7) applies. The time-resolved quenching experiments have been performed on the W1 station which uses the radiation from a 32-pole wiggler. Due to the vertical scattering geometry of the surface diffractometer, the incident beam is polarized parallel to the plane of incidence resulting in a transmission-polarization factor $|\mathbf{t}_{fi}^{\parallel}|^2$ (8). The x-ray energy was chosen to $E_i = 8.27$ keV (D4 experiment) and $E_i = 7.20$ keV (W1 experiment) below the K edge of Cu in order to avoid strong Cu fluorescence scattering. Figure 4 depicts the typical experimental setup: At the W1 station, the energy selection is effected by a Si(111) double monochromator system followed by a total-reflection toroidal mirror which eliminates higher harmonics passed through the monochromator and focuses the beam vertically and horizontally on the sample surface. The D4 spectrometer is furnished with a flat Au-coated mirror and a downstream Ge(111) monochromator. Particular care has been taken in setting the slits before and after the sample: The lower part of Fig. 5 gives the top view of the actual surface of the $Cu_3Au(001)$ single crystal which had an ellipsoidal shape with a long (110) axis of 8 mm and a short (110) axis of 4 mm. The effective beam height covered by the crystal at $\alpha_i/\alpha_c = 1.5$ is less than 100 μm, consequently, the incidence slit σ_{iV} was set between 80 and 100 μm. The two slits σ_{iH} and σ_{fH} horizontal to the sample surface area A_f which is "seen" by the position-sensitive detector. σ_{iH} and σ_{fH} were chosen to be 1 and 1.5 mm, respectively, resulting in a surface area A_f which avoided scattering effects from the edges of the sample (see A_f in Fig. 5). One of the characteristics of this experimental setup[26] is the position-sensitive detector (PSD) which is set at a certain scattering angle $2\theta_B$ and measures an α_f profile of the evanescent scattering between 0 and typically $3-4\alpha_c$. By this the PSD directly provides a depth profile of the near-surface scattering between some 10 Å and several 100 Å depending on the incident angle (Fig. 3).[26,30]

IV. DETAILS OF THE SAMPLE PREPARATION AND SAMPLE ENVIRONMENT

The sample was grown, prepared, and characterized at the Forschungszentrum KfA Jülich-Institut für Festkörper- forschung (IFF).[27] The Cu_3Au single crystal was grown in a special Czochralsky apparatus[28] with a low pulling speed of 3 mm/h in order to avoid the so-called "constitutional supercooling"[28] which would des-

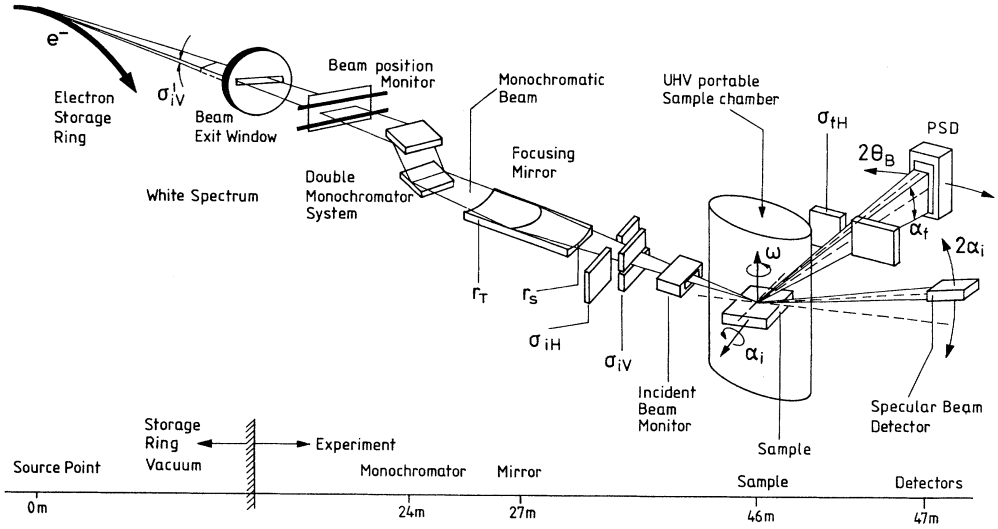

FIG. 4. Depth-controlled grazing-angle diffraction using synchrotron radiation. $\sigma'_{iV} \simeq 0.2$ mrad is the vertical divergence of the x-ray beam; σ_{iH}, σ_{iV}, σ_{fH} are slits; PSD denotes the position sensitive detector. The (distorted) bottom ruler shows the distances realized at the W1 beamline at HASYLAB.

troy the single-crystal growth reaction. Remaining composition gradients and crystal strains were removed by annealing the crystal for 14 days at 800 °C. The actual stoichiometry of the alloy was determined by neutron activation analysis to be $c_{Cu}/c_{Au} = 3.015$. A (001) surface was spark cut and mechanically polished (final polish with 0.1 μm Al_2O_3). Then the sample was brazed onto a Cu plate by baking the assembly in ultrahigh vacuum (UHV) at 600 °C and transferred into the UHV preparation chamber of the FLIPPER II station at HASYLAB, where the final treatment of the sample surface was performed consisting of repeated argon sputtering and annealing at $T = 420$ °C. The subsequent Auger and LEED analysis revealed an atomically clean surface with a well-defined $c(2\times2)$ LEED pattern of the ordered surface.

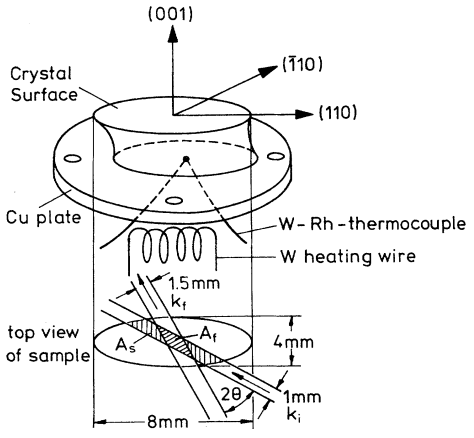

FIG. 5. View of the sample shape and mounting with the heating wire and the thermocouple (top) including the sample areas A_s and A_f as "seen" by the specular and the diffracted beam (bottom). The scattering angle 2Θ is associated with the (100) superlattice reflection.

For the x-ray experiments the sample was mounted via a UHV transfer in a portable UHV chamber which maintained a vacuum of $p \simeq 10^{-10}$ Torr throughout the experiment and allowed free access of the x-ray beam onto the sample surface through a hemispherical Be window. The actual temperature of the sample was monitored by a W-Rh thermocouple which was attached at the backside of the Cu plate (see Fig. 5).

Depth-controlled grazing-angle scattering studies require well-defined incidence and exit angles (α_i, α_f). This, in turn, necessitates that the simple surface is atomically smooth and macroscopically flat on the scale of α_c. The waviness of the surface was checked by the angular widths of the totally reflected x-ray beam at various incidence angles. Figure 6 shows two specular beam profiles as obtained for the incidence angles $\alpha_i = 3.3$ and 6.6 mrad. The only marginal increase in the specular widths compared to the width of the incident beam already tells us that the surface is mirrorlike, a quantitative analysis allowing for instrumental resolution effects gives a surface waviness as measured along the footprint A_s (Fig. 5) of $|\Delta \mathbf{n}_s| = 0.35$–$0.65$ mrad.

V. TEMPERATURE DEPENDENCE OF THE EVANESCENT (100) SUPERLATTICE SCATTERING

The x-ray-scattering study described in this section has been performed on the D4 spectrometer. The evanescent scattering associated with the (100) reciprocal superlattice reflection has been investigated in the temperature

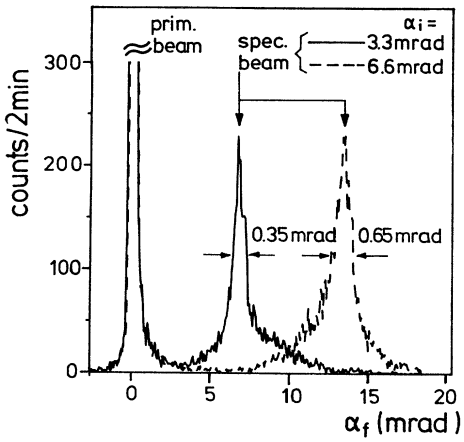

FIG. 6. Specular beam profiles as a function of α_f as measured by the position-sensitive detector at 2Θ for two different incidence angles $\alpha_i = 3.3$ and 6.6 mrad. The widths of the specular profiles give the waviness of the sample along A_s (Fig. 6). The indicated values are corrected for instrumental resolution effects. (Note that the detector was shielded with a 1 mm Al absorber.)

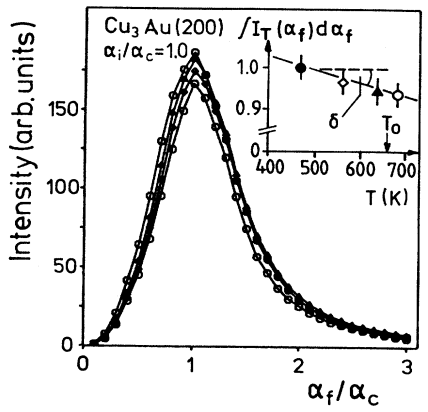

FIG. 7. α_f profiles of the (200) fundamental reflection at $\alpha_i/\alpha_c = 1.0$ for various temperatures. The solid lines are a guide for the eyes. The inset shows the α_f-integrated intensities as a function of the temperature. The slope $\delta = 2M_{\text{eff}} = Q_{\parallel}^2 \langle u_{\text{eff}}^2 \rangle / T$.

range between room temperature (300 K) and 674 K (well above the transition temperature $T_0 = 663$ K). We recorded α_f-resolved spectra and α_f-integrated ω scans of the (100) superlattice reflection and the (200) fundamental reflection at various incidence angles α_i/α_c between 0.5 and 1.5.

The (200) scattering intensity was primarily used to monitor any unusual surface-related Debye-Waller factor and surface-roughening effects associated with the order-disorder phase transition. The α_f profiles of the (200) Bragg scattering exhibit a mild temperature dependence as shown in Fig. 7 for $\alpha_i/\alpha_c = 1.0$. The form factor of a low-order fundamental reflection is, in a good approximation, given by[6]

$$F_{hkl} \simeq 4e^{-M_{\text{eff}}}[(c_{\text{Cu}} f_{\text{Cu}} + c_{\text{Au}} f_{\text{Au}}) + \Delta M (c_{\text{Cu}} f_{\text{Cu}} - c_{\text{Au}} f_{\text{Au}})] \quad (10)$$

with $M_{\text{eff}} = (M_{\text{Cu}} + M_{\text{Au}})/2$ and $\Delta M = M_{\text{Cu}} - M_{\text{Au}}$, where $M_x = \frac{1}{2} Q_{\parallel} \langle u_x^2 \rangle$ and c_x (x=Cu, Au) denote the mean-square thermal amplitude and the average concentration of the Cu and Au atoms, respectively. From the room-temperature bulk values[6]

$$\langle u_{\text{Cu}}^2 \rangle^{1/2} = 0.093 \text{ Å}$$
$$\text{and} \quad (11)$$
$$\langle u_{\text{Au}}^2 \rangle^{1/2} = 0.069 \text{ Å},$$

we can conclude that the second term in $F_{hkl}(10)$ contributes only 1% to the (200) reflection and is thus negligible. From our experimental data we estimate with an uncertainty of 30% that

$$\langle u_{\text{eff}}^2 \rangle / T \simeq 3 \times 10^{-5} \text{ Å}^2/\text{K}$$

in the temperature regime from 473 to 677 K (see inset of Fig. 7) indicating that no significant roughening occurs at the transition temperature. Since the bulk Debye temperature[29] $\theta_D = 277$ K [for the top layers of the $Cu_3Au(001)$ one finds a somewhat lower value[11] $\theta_D^s \simeq 210$ K], the applied high-temperature approximation ($\langle u_{\text{eff}}^2 \rangle / T$ = const) is justified for $T \geq 300$ K and allows the room-temperature value $\langle u_{\text{eff}}^2 \rangle^{1/2}$ to be estimated to be $\simeq 0.095$ Å, which compares reasonably well with the bulk values (11). Due to the large error bar for $\langle u_{\text{eff}}^2 \rangle / T$, we did not attempt to extract any surface effect on the $\langle u_{\text{eff}}^2 \rangle$, on the other hand, we can use $\langle u_{\text{eff}}^2 \rangle / T$ to gauge the Debye-Waller factor of the (100) superlattice peak which is then expected to vary by 2% between $T = 470$ and 670 K. In the subsequent discussion we will ignore this subtle temperature dependence.

Figure 8 shows the ω scan of the (100) Bragg scattering

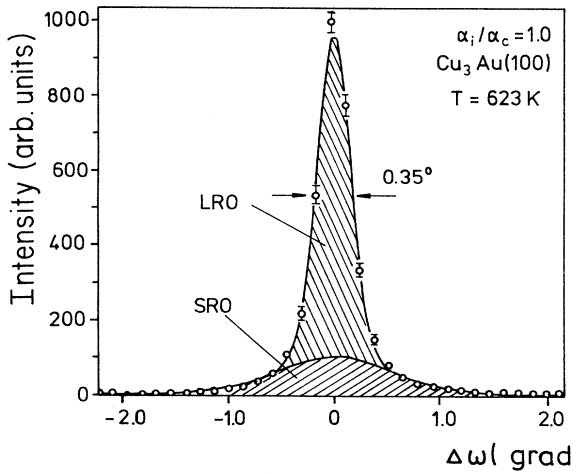

FIG. 8. α_f-integrated intensity distribution around (100) superlattice peak at $T = 623$ K as measured in an ω scan for $\alpha_i/\alpha_c = 1.0$. The solid lines are least-squares fits to the data. The half-width of the LRO contribution is 0.35°.

for $\alpha_i/\alpha_c=1.0$ at $T=623$ K. The peak profile of the ω scan is composed of two contributions, a small Gaussian with a FWHM of 0.35°, which is attributed to near-surface LRO, and a small broad contribution originating from diffuse scattering due to near-surface SRO. The α_f profile at the peak maximum [Fig. 9(a)] shows the characteristic asymmetric line shape typical for evanescent scattering[30] which can be fully understood within the DWBA-scattering theory. Including effects of surface roughness (ρ=average roughness amplitude), surface waviness ($|\Delta\mathbf{n}_s|$=variation of surface normal), and so-called "dead" surface layers, which do not exhibit a noticeable LRO (p=number of surface layers), in Eq. (3) one finds[30-32]

$$I(\alpha_f)\propto\left\langle |T_f e^{-(1/2)(k'_{fz}-k_{fz})^2\rho^2}|^2 \frac{\exp(-q'_z q'^{*}_z\rho^2-2\rho^2/\Lambda^2-2pa_z/\Lambda)}{|1-\exp(iQ'_z a_z)|^2}\right\rangle_{\text{if}}, \tag{12}$$

where k_{fz} is the z component of the wave vector $\mathbf{k}_f$ as observed in the half-space $z<0$ (vacuum) and the brackets $\langle\ \rangle_{\text{if}}$ denote the appropriate average over the actual uncertainties in the incidence and exit angle (as given by beam divergences, the spatial resolution of the PSD, and the waviness $|\Delta\mathbf{n}_s|$ of the illumination sample surface). For the sake of simplicity, we discarded all terms in Eq. (12) which do not depend on α_f and replaced $|t^{\perp}_{fi}|^2$ by

$$|T_f|^2|T_i|^2\cos^2 2\theta_B\ ,$$

which is an excellent approximation as long as $\alpha_{i,f}=O(\alpha_c)$.[30] A missing LRO in the top layers, as described by a nonzero value p, can, for instance, be attributed to an equilibrium surface-induced disorder as discussed in Sec. II or to a quenched surface disorder when the sample is rapidly cooled to room temperature after the high-temperature annealing. Since the LEED measurements disclosed a well-ordered surface, we expect, that $p\simeq 0$ in this case. The solid line in Fig. 9(a) is calculated according to Eq. (12) taking $\rho=10\pm5$ Å, $\Delta n_s=0.2$ mrad, and $p\simeq 1$. First, we note that we obtain a smaller value for Δn_s compared to the $\Delta n_s=0.35-0.65$ mrad from the width of the specular beam which is understood by inspection of Fig. 5: While the reflected beam experiences the waviness of the sample along the footprint A_s, the scattered x-ray beam probes a comparatively small surface area (A_f in Fig. 5) which can be appropriately varied by the two horizontal slits. The fitting parameters ρ and p, which have large error bars, indicate, though, that the surface is reasonably smooth and well ordered. [We note here that, in Eq. (12), we did not take into account an eventual slight miscut of the surface with respect to the (001) direction.]

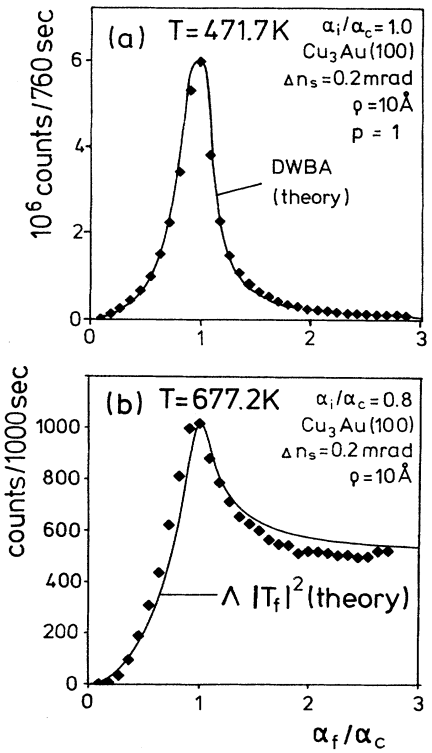

FIG. 9. α_f profiles of the scattering at the (100) and theoretical predictions of the DWBA (solid lines): (a) Bragg intensity observed at $T=471.7$ K, (b) SRO diffuse scattering at $T=677.2$ K. The solid lines are calculated according to Eqs. (12) and (13).

In the first temperature cycle we heated the sample carefully until the LRO near the surface disappeared and obtained, in this way, a rough estimate of the transition temperature and the amount of diffuse scattering in the disordered phase. Figure 9(b) shows the α_f profile of the diffuse scattering at the (100) reciprocal-lattice point at $T=677$ K $=T_0+14$ K and $\alpha_i/\alpha_c=0.8$. The pronounced peak at $\alpha_f/\alpha_c\simeq 1.0$ is solely due to the transmission function of the interface and must not be confused with any remaining LRO. Assuming diffuse scattering with a negligible Q dependence, one gets[30,31]

$$I_{\text{dif}}(\alpha_f)\propto\langle\Lambda|T_f e^{-(1/2)(k'_{fz}-k_{fz})^2\rho^2}|^2\rangle_{\text{if}}\ . \tag{13}$$

The solid line in Fig. 9(b) is calculated from Eq. (13) using the fitted parameters obtained from the Bragg scattering and agrees well with our observation.

The sample was then annealed for 9 h at $T=660.9$ K, which was the first temperature in the ordered phase where we determined α_f profiles of the near-surface LRO. By monitoring the time dependence of the superlattice peak at $\alpha_i/\alpha_c=1.0$, we found that the evanescent (100) intensity saturated at this temperature after approximately 6 h. In the further cooling steps, the (100) Bragg intensity remained constant after 2–3 h. As an example,

we show in Fig. 10 the recorded evanescent Bragg scattering as a function of the elapsed time τ after reduction of the heating current at $\tau=0$. The temperature, which was initially $T_{\text{init}}=T_0-2.2$ K, reached its new value $T_{\text{final}}=T_0-7.8$ K (see also inset in Fig. 10) within a cooling period of $\tau\simeq 8$ min (hatched area) which was accompanied by a drastic increase in the Bragg intensity. For $\tau>8$ min, the superlattice intensity smoothly saturates at its new value (I_2), thereby following, in a good approximation, a simple exponential law (solid line) with a relaxation time obtained from a least-squares fit of $\tau=38.6$ min. The annealing time was therefore chosen to be approximately 3 h. An online data analysis, as shown in Fig. 10, is quite helpful during the actual experiment, since it allows a good estimate of the time required for saturation of the superlattice intensity. Its proper consideration is, as in bulk experiments, indispensable to avoid accidental nonequilibrium LRO measurements. The essence of our experimental observations is summarized in Figs. 11(a) and 11(b), which show α_f profiles of the (100) Bragg intensity in thermal equilibrium at two incidence angles $\alpha_i/\alpha_c=1.0$ and 1.5 for a selection of temperatures below the bulk transition temperature $T_0=663$ K. The data were obtained in the following way: At each temperature we determined, via an α_f-integrated ω scan, the LRO and SRO contribution to the scattering intensity at the (100) reciprocal-lattice vector (as shown by way of example in Fig. 8). From the measured α_f profile, we subtracted the associated SRO contribution [as in Fig. 9(b)] and obtained the LRO part of the α_f profile. This diffuse-scattering correction of the α_f profiles, however, turned out to be very small. (Note the different intensity scales in Fig. 9 for the Bragg and diffuse-scattering profile.) Before we analyze the data quantitatively, we will discuss an interesting feature of these α_f profiles. Mere inspection of the raw data shows quite convincingly that the evanescent superlattice intensity disappears in a completely different way in the different α_f regimes. For $\alpha_f/\alpha_c>1$, the intensity remains virtually unchanged in the entire temperature range until shortly before the transition, where it drops to zero. On the other hand, for $\alpha_f/\alpha_c\leq 1$, we identify a continuous change of the intensity with each temperature step which is more pronounced for $\alpha_i/\alpha_c=1.0$ than for $\alpha_c/\alpha_c=1.5$. This behavior is demonstrated for two different settings of $\Lambda=30$ and 300 Å (Fig. 12). Since α_f crucially determines the surface sensitivity, we interpret this observation as surface-mediated phenomenon, where the (001) surface induces a continuous change of the LRO parameter in agreement with the conclusions drawn from LEED and SPLEED measurements.[33] This demonstrates quite convincingly that the α_i profiles of the LRO intensity allow the simultaneous observation of the discontinuous bulk order-disorder transition and the continuous loss of LRO near the surface. From this analysis we find within an uncertainty of 0.5 K that the transition temperature T_0 is independent from the distance z; in other words, there is no surface-induced new phase transition.

For a quantitative analysis of the observed evanescent Bragg scattering, we plot the data $I_\Lambda(t)$ associated with various scattering depths Λ (between 17 and 500 Å) versus the reduced temperature $t\equiv(T_0-T)/T_0$ on a

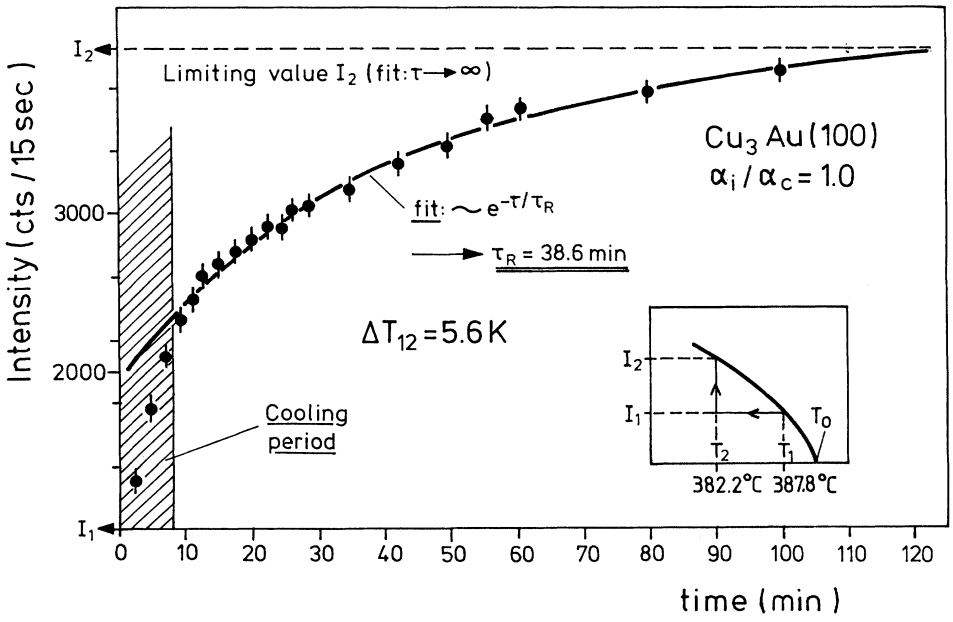

FIG. 10. Time dependence of the α_f-integrated evanescent superlattice intensity at $\alpha_i/\alpha_c=1.0$ upon cooling in the presence of an ordered bulk. The start and end temperatures are explained in the inset. The hatched area indicates the time required for the sample to achieve its new temperature. The solid line is a least-squares fit.

double-logarithmic scale (Fig. 13). The intensities $I_\Lambda(t)$ exhibit a general trend.

(a) Starting with a mild temperature dependence far away from T_0, they enter in a marked T dependence close to T_0 which ends up in an asymptotic power-law behavior as indicated by the solid lines with slope $2\beta_\Lambda$,

$$I_\Lambda(t) \propto |t|^{2\beta_\Lambda} . \tag{14}$$

(b) The asymptotic power law becomes more pronounced, the more surface sensitive we tune the scattering depth. The underlying rule is disclosed quite simply by plotting β_Λ versus $1/\Lambda$ (Fig. 14). All β_Λ values lie on a straight line through the origin; thus,

$$\beta_\Lambda = \xi_m / \Lambda . \tag{15}$$

It is interesting to note that the experimental value $\beta_1 = 0.77$ as deduced from SPLEED is just comparable to the β_Λ values for small values of Λ (see arrow in Fig. 14), whereas for large Λ the exponent β_Λ tends to zero, which is typical for first-order phase transitions. In this way, Fig. 14 displays very nicely the smooth depth transition from the surface-induced continuous behavior of the long-range order to the discontinuous bulk behavior. The length ξ_m is the slope of the solid line in Fig. 14,

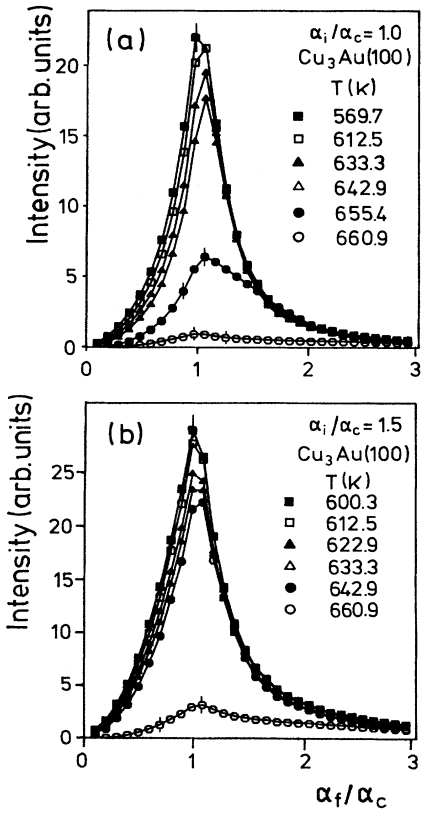

FIG. 11. α_f profiles of the (100) superlattice Bragg intensity at various temperatures below the transition temperature T_0, (a) for $\alpha_i/\alpha_c = 1.0$, (b) for $\alpha_i/\alpha_c = 1.5$. The solid lines are a guide for the eyes.

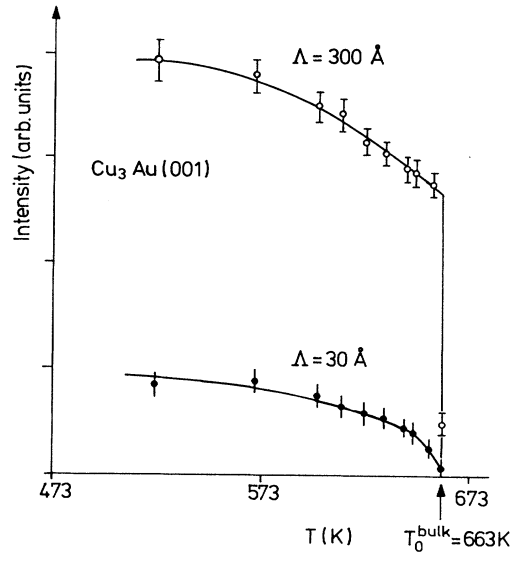

FIG. 12. Temperature dependence of the evanescent superlattice intensity at two different scattering depths $\Lambda = 30$ and 300 Å. (The solid lines are a guide for the eyes.)

$$\xi_m = (13.1^{+1.1}_{-2.5})\ \text{Å} \tag{16}$$

with the error bars resulting from the indicated dashed lines in Fig. 14. Two questions arise from this observation.

(a) "Why do the exponents in the asymptotic power-law regime scale with $1/\Lambda$"

(b) "What is the meaning of the microscopic length ξ_m?"

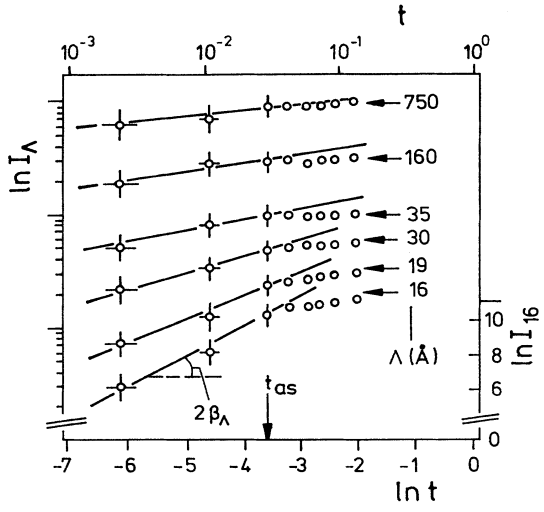

FIG. 13. Evanescent superlattice intensities I_Λ associated with scattering depth Λ as a function of the reduced temperature $t \equiv (T_0 - T)$ on a double-logarithmic scale. t_{as} denotes the onset of the asymptotic regime, $2\beta_\Lambda$ denotes the near-surface "critical exponent" (see main text).

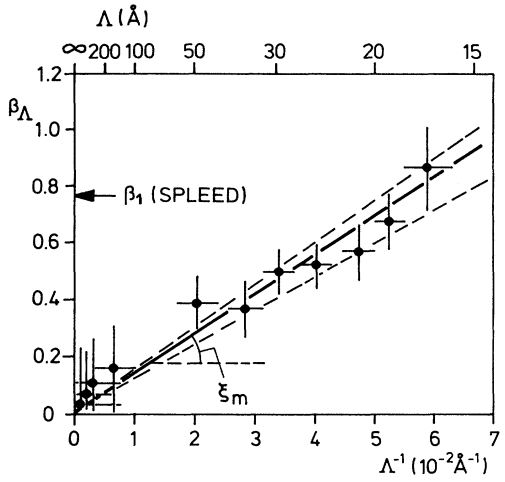

FIG. 14. Experimental values β_Λ deduced from Fig. 13 as a function of $1/\Lambda$. The arrow indicates the surface exponent β_1 as observed by SPLEED (Ref. 13). The solid line follows from a linear regression giving a slope $\xi_m = 13.1$ Å. The two dashed curves determine the error bars $^{+1.1}_{-2.5}$ Å of ξ_m.

We will show in what follows that both features are intimately related to a wetting phenomenon associated with the first-order bulk transition.

For systems where the surface order is driven by the bulk order ("ordinary systems"), the mean-field solution of $m(z,t)$ assumes, according to Lipowsky and Speth, the asymptotic form as shown in Fig. 2(b) which can be written in the convenient analytic form

$$m(z,t)=\tanh\left[\frac{z-L(t)}{\xi_\perp}\right] \tag{17}$$

close to the transition temperature ($T \le T_0$), where $L(t)$ denotes the position of the interface which is given by (1) and $\xi_\perp$ its width or roughness which has a very smooth temperature dependence. For small values of L, the interface is assumed to be smooth because it experiences the potential of the ordered bulk, accordingly, $\xi_\perp \simeq \xi_b = 0(a_z)$, very close to the phase transition where L is of mesoscopic size, the beginning interfacial fluctuations eventually tend to increase $\xi_\perp$ slightly with temperature,[18]

$$\xi_\perp \propto \xi_b \sqrt{\ln|1/t|}\ .$$

The temperature dependence of the evanescent intensity associated with a fixed scattering depth Λ is given by

$$I_\Lambda(t) \propto \left| \int_0^\infty m(z,t) e^{-z/\Lambda} dz \right|^2 , \tag{18}$$

and provides the Laplace transformed image of the order-parameter profile $m(z,t)$ close to the free surface. In the following we study the leading behavior of the wetting transition, namely, the growth of a disordered surface layer with an effective thickness $L(t)$ (1); thus, by ignoring the width $\xi_\perp$ of the order-disorder wall,

$$m(z,t)=\Theta(z-\xi_d \ln|1/t|)\ . \tag{19}$$

$\Theta(x)$ is the Heaviside function. Inserting $m(z,t)$ (19) into Eq. (18), we get

$$I_\Lambda(t) \propto \left| \int_0^\infty e^{-z/\Lambda} \Theta(z-\xi_d \ln|1/t|) dz \right|^2 = |t|^{2\xi_d/\Lambda} \tag{20}$$

and recover the experimentally observed power law with a $1/\Lambda$-scaling behavior of the exponent. This power-law behavior (20) of evanescent Bragg scattering is apparently a direct indicator of a wetting transition. By comparison of Eq. (20) with Eqs. (14)–(16), we can identify the microscopic length ξ_m as the growth amplitude of the disordered phase and get our final experimental result

$$L(t)=(13.1^{+1.1}_{-2.5})\ \text{Å}\ \ln|1/t|\ . \tag{21}$$

Since we are dealing with a first-order phase transition, ξ_d is expected to remain finite on a microscopic range throughout the entire temperature regime; the obtained value of approximately $3a_z$ is thus quite reasonable. Our result may be compared with the Monte Carlo calculations by Gompper and Kroll[19] who also find a logarithmic growth of the wetting layer with $\xi_d \simeq 7.5$ Å. In view of the uncertainties in our experimental value and of the open parameters in the Monte Carlo simulations, we consider this as a reasonable agreement between theory and experiment. Note that the Monte Carlo calculations do, in particular, not account for any surface-induced changes in the coupling constants. This may also be the reason for the large discrepancy between the calculated value of β_1 and the experimental one as discussed above. An independent experimental measurement of β_1 with evanescent x-ray would therefore be highly desirable.

In principle, it should be possible to extract β_1 from evanescent x-ray data such as ours. For this purpose we consider the temperature regime $t \ge t_{as}$ (Fig. 13) where the onset of the surface-induced disorder occurs. The associated z profile of the LRO parameter is then described by [Fig. 2(a)]

$$m(z,t)=1-[1-m(0,t)]e^{-z/\xi}\ ,$$

(ξ is the bulk correlation length), which leads to

$$I_\Lambda(t)/I_\Lambda(\infty)=1-\{2\xi[1-m(0,t)]\}/\Lambda\ , \tag{22}$$

where $I_\Lambda(\infty)$ is the evanescent intensity far away from T_0. In Fig. 15 the quantity $[1-I_\Lambda(t)/I_\Lambda(\infty)]$ is plotted versus $1/\Lambda$ for three different reduced temperatures t and indeed exhibits the expected linear relations (solid lines). The associated slopes provide, according to Eq. (22), the quantity $\{2\xi[1-m(0,t)]\}/\Lambda$ and thus the temperature dependence of the top-layer LRO parameter $m(0,t) \propto |t|^{\beta_1}$. However, in order to extract any reliable surface exponent β_1, a detailed study of the quantity $[1-I_\Lambda(t)/I_\Lambda(\infty)]$ in a wider temperature range is necessary. A related discussion of this is also found in Ref. 19 where the feasibility of such experiments is analyzed in view of the results from renormalization-group calculations. There one finds that the surface-modified LRO decays as

$$\Delta m_z(t)=\Delta m_0(t) e^{-\lambda_1 z}$$

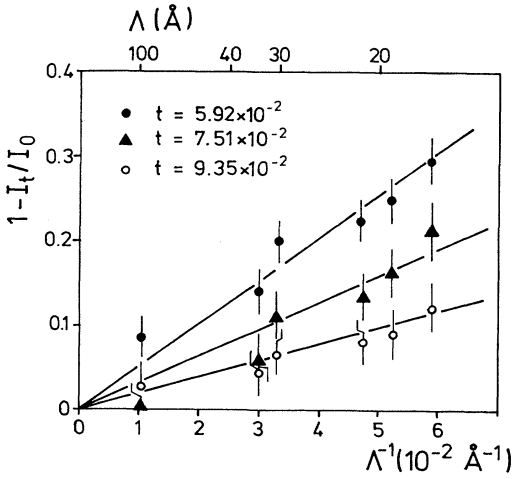

FIg. 15. Experimental test of the relation (22) in the regime $t > t_{as}$ for three different reduced temperatures. The quantity $1-I_t/I_\infty$ is plotted vs $1/\Lambda$.

with distance from the surface, where λ_1 is a nonuniversal inverse decay length which turns out, in the framework of their model, to be $\lambda_1 = 1.6$ (reciprocal units) for the $Cu_3Au(001)$ surface. The temperature dependence of $\Delta m_0(t)$ is accessible to evanescent x-rays if $\lambda_1 \Lambda < 1$, thus for small values of α_i, where the scattering depth Λ is smallest.

We finally indicate how a finite interfacial width $\xi_\perp \simeq \xi_d$ would be detectable in evanescent x-ray scattering. By evaluating the Laplace transform (18) with $m(z,t)$ (17), we get, as long as $\epsilon \equiv \xi_\perp/\Lambda$ is small compared to 1 and $L(t) \propto \ln|1/t|$,

$$I_\Lambda(t) \propto |t|^{2\beta_\Lambda}[1-\epsilon|1/t|^{1+\epsilon}+O(\epsilon^2)]$$

with a leading correction term proportional to $\xi_\perp$. Thus, a nonzero $\xi_\perp$ is observable as a deviation of $I_\Lambda(t)$ from the simple power-law behavior in the asymptotic regime for small values of t. It should be noted, however, that $I_\Lambda(t)$ is also expected to deviate from the power law for small t, as soon as the thickness of the wetting layer becomes thick enough to allow the long-ranging interactions to enter the scenario. Then, the logarithmic delocalization (2) of the order-disorder interface turns into

$$L(t) \propto |t|^{-1/3} ,$$

which causes a crossover to a stretched exponential decrease of the evanescent superlattice scattering.

VI. NEAR-SURFACE RELAXATION TIMES

In this section we discuss some measurements on the near-surface LRO relaxation times when the sample is quenched from above T_0. We shall see that the time scale, which the evanescent superlattice reflection requires to develop upon lowering temperature, provides some additional evidence for the near-surface ordering mechanism.

The time dependence of the Cu_3Au bulk LRO has been extensively studied experimentally[34–38] as well as theoretically.[39,40] We refer the reader to some excellent review articles.[41] The focus of interest has been the late stage of the so-called "coarsening regime," where the line shape of the superlattice reflection shows a universal scaling behavior. The time required for the saturation of the LRO is very long, typically some 10^5–10^6 s. The associated bulk intensity can be satisfactorily fitted by[42]

$$I(\tau) = I_\infty(1-e^{-\tau/\tau_K}) , \tag{23}$$

where τ_K is the so-called "Kramers time," which is a measure for the escape rate from the disordered in the ordered state.[43] τ_K depends on $\Delta T \equiv T_0 - T_{\text{final}}$ (T_{final} is the end temperature of the quench), the so far performed experimental values range from 25 min for $\Delta T = 10$ K to some 100 min for smaller ΔT ("critical slowing down").[36]

Theoretical studies of the temporal growth of wetting layers are reviewed by de Gennes.[44] Recently, Lipowsky[45] considered the influence of short- and long-range interactions on the growth characteristics of wetting layers when the temperature is raised from $T < T_0$ to $T = T_0$. The first experimental evidence of the time dependence of the surface LRO has meanwhile become available from LEIS, LEED,[46] and x-ray-scattering experiments.[47] It turns out that the typical relaxation time τ depends sensitively upon the crystal surface and the associated surface segregation phenomena: At the (100) surface, τ of the top layers is reported to be around 10 s and thus a factor 10^5 smaller than the bulk value.[46] The ideal compositional termination of this surface obviously entails this rapid ordering of the (001) top layer. At the (110) and (111) surfaces, a temperature-dependent surface enrichment of Au occurs,[46,48] the associated LRO relaxation times of the surface superlattice reflection are found to be comparable to or even longer than the bulk values. Apparently, the establishment of surface LRO requires there, due to surface segregation, a long-ranging transport of the atoms from and to the surface. In view of this "sluggish" behavior of the (011) and (111) surface, the reported surface-induced ordering at the $Cu_3Au(111)$ surface,[49] which caused some confusion among the community, is presumably a nonequilibrium phenomenon.

This complicated situation at the surface of binary alloys becomes a little more transparent if one realizes that the depth profile of the LRO parameter $m(z)$

$$m(z) = \frac{3}{4}\left[\frac{r_\alpha(z)-c_{Cu}(z)}{1-c_{Cu}(z)}\right] + \frac{1}{4}\left[\frac{r_\beta(z)-c_{Au}(z)}{1-c_{Au}(z)}\right] , \tag{24}$$

is governed by both the depth profiles of the occupation probabilities $r_\gamma(z)$ ($\gamma = \alpha,\beta$) and of the actual concentration $c_x(z)$ of the constituent x (x=Cu, Au). If $c_x(z)$ changes in the temperature regime around the order-disorder transition temperature, this affects $m(z)$ and the temporal relaxation of $m(z,\tau)$ upon a temperature quench, since $r_\gamma(z,\tau_r)$ and $c_x(z,\tau_c)$ have different relaxation processes with different relaxation times which interfere with an effective time dependence of $m(z)$. At the (010) surface of Cu_3Au, $c_x(z)$ does not change with temperature in our experimental temperature regime; thus,

one has there the possibility to study the relaxation process of the relevant ordering density $r_y(z)$.

In the following we present some first experimental data on the relaxation time near the (001) surface. Due to the presence of the (001) surface, $\tau_K(z,\Delta T)$ will depend, as we shall see, on the distance to the surface. The time-resolved quench experiments were performed with Wiggler radiation. We did not investigate the dependence of τ_K upon ΔT, but focused on the depth dependence of τ_K. In one experiment we quenched the sample from $T_{\text{init}}=T_0+10$ K to $T_{\text{final}}=T_0-30$ K ("deep quench") and observed within the first hour, the time development of the short- and long-range order for two different incidence angles $\alpha_i=0.6\alpha_c$ and $1.1\alpha_c$. For these measurements the PSD was turned by 90° for a $\mathbf{Q}_\parallel$ Ewald scan through the (001) reciprocal-lattice point which is, in a very good approximation, a radial scan. Note that, in this geometry, the σ_{fH} slit, after the sample, now acts as a pinhole (Fig. 4). The PSD was aligned to cover an α_f range around $1.3\alpha_c$ which corresponds to $\Lambda=40$ and 300 Å for the two incidence angles (Fig. 3). After the reduction of the heating current, the temperature of the sample achieved its new value after approximately 8 min. The radial intensity distribution was measured in 2-min intervals. Figure 16 illustrates, by way of example, the observations for $\alpha_i/\alpha_c=1.1$ at three different times after the quench together with theoretical curves: shortly after the temperature drop, strong short-range order fluctuations appear [Fig. 16(a)] on top of which the near-surface long-range order develops [Figs. 16(b) and 16(c)]. The solid lines, which are the results of a least-squares fitting procedure, are composed out of two contributions, a broad line attributed to SRO and a smaller Gaussian curve with temporally decreasing width associated with LRO. Figure 17 summarizes how the radial intensity and the radial profiles evolve for the two different incidence angles. This profile analysis allows one to plot the time dependence of the LRO intensity. In the initial stage of the quench, the time dependence of the quantity

$$\chi_\Lambda(\tau)\equiv I_\Lambda(\tau)/I_\Lambda(\infty)$$

(Fig. 18) can be very well described by exponential curves for both settings of Λ (solid lines), while, at a later stage, a somewhat smoother time dependence is observable (as indicated by the dashed line). The important observation, which we will focus on in the following, is that the LRO associated with the large scattering depth of $\Lambda=300$ Å ($\alpha_i/\alpha_c=1.1$) outcrops first with a time constant $\tau_K\simeq 6.5$ min followed by the surface LRO associated with $\Lambda=40$ Å ($\alpha_i/\alpha_c=0.6$), which has noticeably larger initial time constant of $\tau_K=16$ min. This near-surface relaxation behavior may be understood from the equilibrium properties of the surface LRO: All equilibrium experiments performed at the $Cu_3Au(001)$ surface reveal a so-called "ordinary" behavior of the surface LRO, i.e., the surface favors disorder and the surface LRO is driven by the bulk. Thus, any surface LRO can only develop in the presence of LRO in the bulk of the system. Consequently, one would expect that, in a temperature quench from the fully disordered state, the surface LRO should always lag temporarily behind the bulk LRO. A quantitative description of the near-surface relaxation appears complex. Even in a simplified heuristic model one has to account for a disordered surface region of which the thickness $L(\tau)$ decreases with time, until, finally, it reaches the equilibrium situation as shown in Fig. 2(a). While the bulk relaxation is characterized by a Kramers time τ_K^b, the disordered surface region exhibits an "after" relaxation on top of the actual bulk long-range order which may be described by $\tau_K^s(z)$. In a first simplification of the model, we take τ_K^s as an effective relaxation time averaged over the disordered surface region (Fig. 19). A straightforward calculation then yields the quantity

$$\begin{aligned}\Delta\chi_{12}(\tau)&\equiv\chi_{\Lambda_1}(\tau)-\chi_{\Lambda_2}(\tau)\\&=(e^{-\tau/\tau_K^b}-e^{-\tau/(\tau_K^b+\tau_K^2)})\\&\quad\times(e^{-L(\tau)/\Lambda_1}-e^{-L(\tau)/\Lambda_2}),\end{aligned}\tag{25}$$

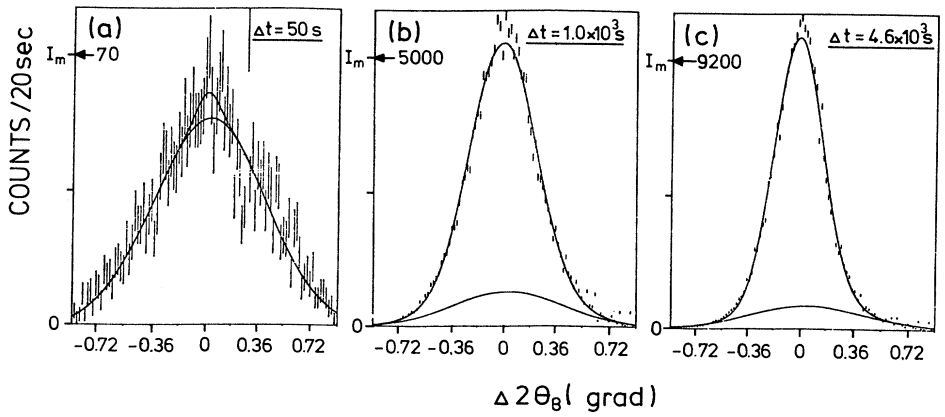

FIG. 16. Experimental line shapes of the (100) scattering intensity and results from a peak shape analysis at three different times after the temperature quench $\Delta T=30$ K. The broad component is ascribed to near-surface short-range order, the small Gaussian component to surface LRO.

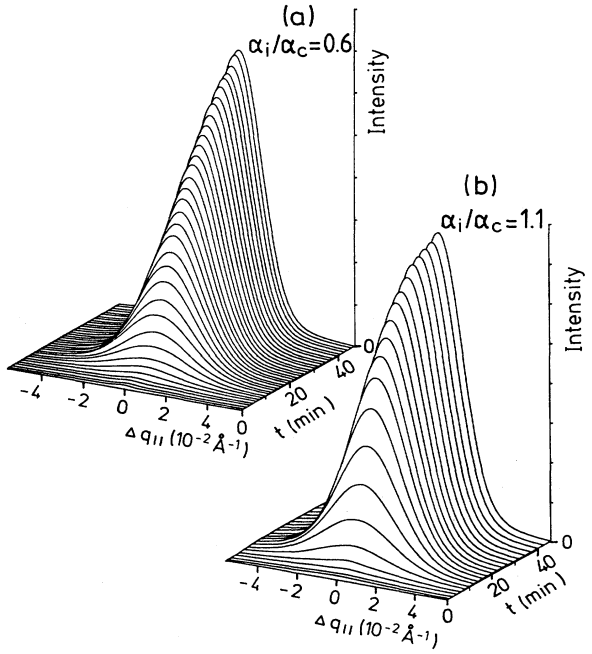

FIG. 17. Time evolution of the radial intensity profiles after the quench from the disordered bulk for two incidence angles $\alpha_i/\alpha_f=0.6$ and 1.1. $\Delta q_{\parallel}$ is the reciprocal distance to the (100) reciprocal-lattice vector. The intensity scale is arbitrary.

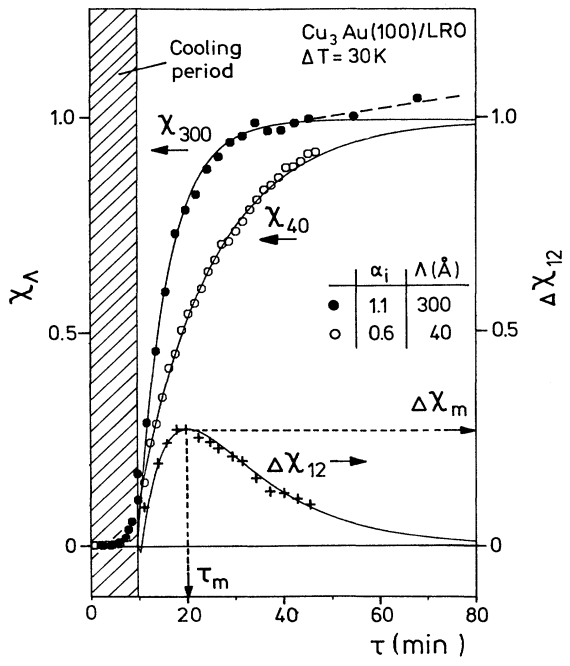

FIG. 18. The quantities $\chi_\Lambda \equiv I_\Lambda/I_\infty$ for $\Lambda=300$ and 40 Å and $\Delta\chi_{12}\equiv\chi_{300}-\chi_{40}$ as a function of time after a quench from T_0+10 K to T_0-30 K. The solid lines are the result of a least-squares fit. The dashed curve indicates the deviation from the exponential curve.

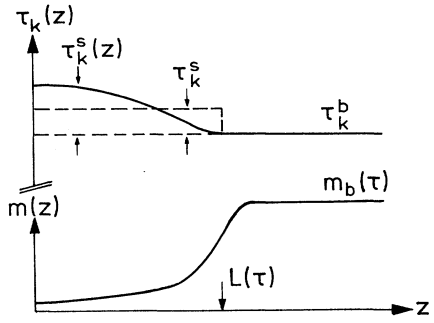

FIG. 19. Possible near-surface relaxation scenario. (For explanation see main text.)

which vanishes for $\tau=0$ and ∞ and is expected to exhibit a maximum at a time τ_m which depends on τ_K^b, τ_K^s, and $L(\tau)$. The observed values of $\Delta\chi_{12}\equiv\chi_{300}-\chi_{40}$ are included in Fig. 18 and indeed exhibit such a maximum ($\Delta\chi_m$) at $\tau_m=20.8$ min. From the experiments performed at thermal equilibrium, we know that $L(t)$ ranges from a microscopic to a mesoscopic scale depending on the reduced temperature; thus, we anticipate a similar range for $L(\tau)$. In order to estimate the order of magnitude of $L(\tau)$, we replace $L(\tau)$ in Eq. (25) by an effective disordered region L and find, within this approximation, that the maximum $\Delta\chi_m$,

$$\Delta\chi_m \propto e^{-L/\Lambda_1}-e^{-L/\Lambda_2} \tag{26}$$

is achieved at

$$\tau_m=(\tau_K^b+\tau_K^s)\frac{\ln(1+\gamma)}{\gamma},\quad \gamma=\tau_K^s/\tau_K^b\ , \tag{27}$$

when the bulk LRO has its biggest temporal lead over the lagging surface LRO. In this crude relaxation model we expect τ_m to be independent of Λ, while information on the length scale L is obtained from the dependence of the maximum $\Delta\chi_m$ upon the scattering depth Λ (26).

For an experimental estimate of L, time-resolved α_f profiles of the (100) Bragg scattering were measured during a quench from $T_{\text{init}}=T_0+10$ K to $T_{\text{final}}=T_0-36$ K and depth profiles of the near-surface relaxation behavior of the surface LRO between $\Lambda=20$ and 300 Å were obtained in this way. The results for $\chi_\Lambda(\tau)$ for $\Lambda=20$, 35, 100, and 220 Å are summarized in Fig. 20(a) together with the exponential fits and the associated τ_K values [see inset of Fig. 20(a)], which increase very distinctly with decreasing scattering depth. The derived quantities $\Delta\chi_{12}(\tau)$ for $\Lambda_1=220$ Å and $\Lambda_2=20$, 35, and 100 Å [Fig. 20(b)] display maxima $\Delta\chi_m(\Lambda_2)$, which becomes more and more pronounced as the surface sensitivity is increased, in agreement with Eq. (26) which can be used now to estimate L. By solving Eq. (26) numerically, we find

$$L\simeq 10a_z\ , \tag{28}$$

which lies, as expected, in the mesoscopic regime ("lattice constant $\ll L \ll$ crystal"). Thus, within the first minutes

of the quench, an average surface layer of thickness $10a_z$ starts ordering with a time constant which is noticeably larger than the bulk value. The time τ_m (27) when the maximum occurs during this quench is found to vary softly with Λ between 17.6 min for $\Lambda_2=20$ Å to 14.7 min for $\Lambda_2=100$ Å and appears, thus, not totally independent from Λ as assumed in the near-surface scenario. Note on the other hand that, in the first quench with a slightly different ΔT, we obtained $\tau_m=20.8$ min. The fact that

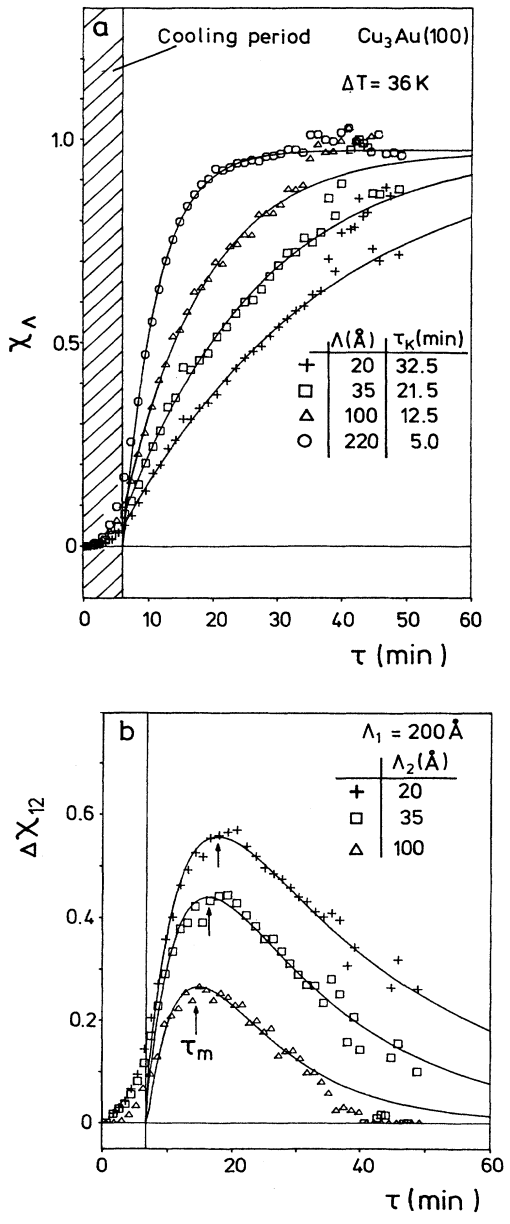

FIG. 20. Results from the time-resolved α_f profiles of the (100) superlattice intensity after a quench from T_0+10 K to T_0-36 K. (a) χ_Λ vs time for $\Lambda=20$, 35, 100, and 220 Å. (b) $\Delta\chi_{12}$ for $\Lambda_1=220$ Å and $\Lambda_1=20$, 35, and 100 Å vs time. The solid lines are least-squares fit to the data. The arrows indicate the elapsed time τ_m when the maximum occurs.

τ_m (27) depends on ΔT is not surprising since τ_K^b and also, presumably, τ_m^s are functions of ΔT. From the observed depth dependence of τ_K and the result (28), we conclude that our depth- and time-resolved quench experiments add further independent evidence that the $Cu_3Au(001)$ surface shows "surface-induced disorder (SID)." The phenomenological dynamics of the surface LRO is governed by the Langevin equation

$$\frac{\delta m(z,\tau)}{\delta\tau}=-\tau_K^{-1}(z)\frac{\delta F(m)}{\delta m}$$

with F as the free energy of the semi-infinite system[15] and τ_K^{-1} as the relaxation rate associated with a nonconserved surface LRO. Clearly, more time-resolved surface-sensitive measurements of $\tau_K(z)$ could be useful as an experimental input into such theoretical models.

VII. FINAL REMARKS

The x-ray experiments described here together with the other surface work provides a consistent picture of the ordering phenomena near the $Cu_3Au(001)$ surface when the bulk order-disorder transition temperature is approached. It should be emphasized that the apparent simplicity of these surface phenomena is due to the absence of noticeable surface-segregation effects at this surface. This fact allows, first of all, that x-ray experiments can be performed in a reasonable time, because of the associated short relaxation times, and secondly a straightforward interpretation of near-surface Bragg intensities. It should be noted that a continuous change of a surface superlattice intensity can be related to a continuous change in the surface LRO parameter in a simple way only in that case, where the bulk stoichiometry is maintained at the surface, i.e., when $c_x(z)$ in $m(z)$ (24) do not change within the temperature regime under investigation. If a temperature-dependent surface segregation occurs, as, e.g., in the case of the $Cu_3Au(011)$ and $Cu_3Au(111)$ surfaces, the temperature dependences of $r_y(z)$ and $c_x(z)$ overlap and result in a rather complicated behavior.

The observation of a disordered ("wet") surface layer, which grows logarithmically as the first-order bulk phase transition is approached, is so far the most direct experimental confirmation of the theoretical concept of SID as proposed by Lipowsky.[15] One expects this so-called "ordinary" surface phenomenon to occur if the surface couplings between the constituents of the alloy are not so much enhanced compared to the bulk that they do not compensate the reduction of the order parameter at the surface due to the broken bonds. This surface-enhancement factor $\Delta_s\equiv J_s/J$ (J_s is the nearest-neighbor interaction at the surface, J is the one in the bulk) is not known so far and enters the theory as a free parameter. A direct measurement of these surface couplings would

therefore be highly desirable. Short-range-order diffuse x-ray scattering from the evanescent wave field provides the possibility of determining surface-induced Cowley short-range order parameters which are a direct measure of the pairwise interaction potentials close to the surface. This weak diffuse evanescent scattering is accessible today[50] using the intense Wiggler radiation provided by modern synchrotron radiation laboratories. Due to the broken translational symmetry at the surface and the complicated effects of surface segregation, the proper theoretical interpretation is not straightforward, nonetheless, first attempts to attack this important problem have already been reported.[51]

ACKNOWLEDGMENTS

The assistance of Andreas Lied and Francois Grey during the experiments was greatly appreciated. We thank W. Gudat and Sybille Krummacher for making the Cu_3Au single crystal available to us, the HASYLAB staff for the hospitality and the technical support during the experiments, and the Riso "surface science" group for technical assistance. The authors benefited from many inspiring and clarifying discussions with Reinhard Lipowsky and H. Wagner. This work was supported by the Bundesminister für Forschung und Technologie under project Nos. 03PEILMU2 and 05490CAB.

[1]H. Dosch, L. Mailänder, A. Lied, J. Peisl, F. Grey, R. L. Johnson, and S. Krummacher, Phys. Rev. Lett. **60**, 2382 (1988).
[2]L. Mailänder, H. Dosch, J. Peisl, and R. L. Johnson, Phys. Rev. Lett. **64**, 2527 (1990).
[3]B. E. Warren, *X-Ray Diffraction* (Addison-Wesley, Reading, MA, 1969).
[4]J. M. Cowley, Phys. Rev. **77**, 669 (1950); J. Appl. Phys. **21**, 24 (1950).
[5]S. C. Moss, in *Local Atomic Arrangements Studied by X-Ray Diffraction,* edited by J. B. Cohen and J. E. Hilliard (Gordon and Breach Science, New York, 1966).
[6]D. R. Chipman, Phys. Rev. **27**, 739 (1956).
[7]K. Binder, W. Kinzel, and W. Selke, J. Magn. Mater. **31**, 1445 (1983).
[8]Z. W. Wilchinsky, J. Appl. Phys. **15**, 806 (1944).
[9]B. E. Warren and R. Chipman, Phys. Rev. **75**, 1629 (1949).
[10]V. S. Sundaram, B. Farrell, R. S. Alben, and W. D. Robertson, Phys. Rev. Lett. **31**, 1136 (1973).
[11]V. S. Sundaram, R. S. Alben, and W. D. Robertson, Surf. Sci. **46**, 653 (1974).
[12]E. G. McRae and R. A. Malic, Surf. Sci. **148**, 551 (1984).
[13]S. F. Alvarado, M. Campagna, A. Fattah, and W. Uelhoff, Z. Phys. B **66**, 103 (1987).
[14]J. M. Sanchez and J. L. Moran-Lopez, Phys. Rev. B **32**, 3534 (1985); Surf. Sci. **157**, L297 (1985).
[15]R. Lipowsky, Phys. Rev. Lett. **49**, 1575 (1982); Z. Phys. B **51**, 165 (1983); J. Appl. Phys. **55**, 2485 (1984).
[16]R. Lipowsky and W. Späth, Phys. Rev. B **28**, 3983 (1983).
[17]R. Lipowsky, D. M. Kroll, and R. K. P. Zia, Phys. Rev. B **27**, 4499 (1983).
[18]R. Lipowsky, Ferroelectrics **73**, 69 (1987).
[19]D. M. Kroll and G. Gompper, Phys. Rev. B **36**, 7078 (1987); G. Gompper and D. M. Kroll, *ibid.* **38**, 459 (1988).
[20]T. Buck, G. H. Wheatley, and L. Marchut, Phys. Rev. Lett. **51**, 43 (1983).
[21]K. Binder, D. P. Landau, and D. M. Kroll, Phys. Rev. Lett. **56**, 2272 (1986).
[22]*International Tables for X-Ray Crystallography* (Kynoch, Birmingham, 1985), Vol. III.
[23]G. H. Vineyard, Phys. Rev. B **26**, 4146 (1982).
[24]S. Dietrich and H. Wagner, Z. Phys. B **56**, 207 (1984).
[25]M. Born and E. Wolf, *Principles of Optics* (Pergamon, New York, 1986).
[26]H. Dosch, B. W. Batterman, and D. C. Wack, Phys. Rev. Lett. **56**, 1144 (1986).
[27]The growth and the preparation was done by W. Uelhoff and A. Fattah at KFA-IFF.
[28]W. Uelhoff, Festkorperprobleme **27**, 241 (1987); H. Wenzl, A. Fattah, and W. Uelhoff, J. Cryst. Growth **36**, 319 (1976).
[29]S. L. Quimby, Phys. Rev. **95**, 916 (1953).
[30]H. Dosch, Phys. Rev. B **35**, 2137 (1987).
[31]B. Vidal and P. Vincent, Appl. Opt. **23**, 1794 (1984).
[32]S. K. Sinha, E. B. Sirota, S. Garoff, and H. B. Stanley, Phys. Rev. B **38**, 2297 (1988).
[33]Note that the data shown in Fig. 12 are the Fourier-Laplace transform of the order-parameter profile $m(z)$.
[34]E. Nagy and I. Nagy, J. Phys. Chem. Solids **23**, 1605 (1962); H. Elkholy and E. Nagy, *ibid.* **23**, 1613 (1962).
[35]M. Sakai and D. E. Mikkola, Metall. Trans. **2**, 1635 (1971).
[36]T. Hashimoto, T. Miyoshi, and H. Ohtsuka, Phys. Rev. B **13**, 1119 (1976); T. Hashimoto, K. Nishimura, and Y. Takeuchi, J. Phys. Soc. Jpn. **45**, 1127 (1978).
[37]Y. Noda, S. Nishihara, and Y. Yamada, J. Phys. Soc. Jpn. **53**, 4241 (1984).
[38]S. E. Nagler, R. F. Shannon, C. R. Harkless, M. A. Singh, and R. M. Nicklow, Phys. Rev. Lett. **61**, 1859 (1988).
[39]K. Binder and D. Stauffer, Phys. Rev. Lett. **33**, 1006 (1974).
[40]Z. W. Lai, Phys. Rev. B **41**, 9239 (1990).
[41]J. D. Gunton, M. San Miguel, and P. S. Sahni, in *Phase Transitions and Critical Phenomena,* edited by C. Domb and J. L. Lebowitz (Academic, London, 1983); K. Binder and D. W. Heerman, in *Scaling Phenomena in Disordered Systems,* edited by R. Paym, and A. Skieltorp (Plenum, New York, 1985).
[42]S. Nishihara, Y. Noda, and Y. Yamada, Solid State Commun. **44**, 1487 (1982).
[43]J. S. Langer, Ann. Phys. **41**, 108 (1967).
[44]P. de Gennes, Rev. Mod. Phys. **57**, 827 (1985).
[45]R. Lipowsky, J. Phys. A **18**, L585 (1985).
[46]E. G. McRae and T. M. Buck, Surf. Sci. **227**, 67 (1990).
[47]X. M. Zhu, I. K. Robinson, E. Velig, H. Zabel, J. A. Dura, and C. P. Flynn, J. Phys. (Paris) Colloq. **50**, C7-283, (1989).
[48]J. M. McDavid and S. C. Fain, Jr., Surf. Sci. **52**, 161 (1975).
[49]X. M. Zhu, R. Feidenhans'l, H. Zabel, J. Als-Nielsen, R. Du, C. P. Flynn, and F. Grey, Phys. Rev. B **37**, 7157 (1988); one should mention that the authors erroneously discuss their results in the framework of bulk-critical phenomena.
[50]H. Dosch, J. Peisl, and R. L. Johnson (unpublished).
[51]D. M. Kroll and H. Wagner, Phys. B **42**, 6531 (1990).